Method for the posture control of bionic mechanical wheel-legged vehicles in hilly and mountainous areas

Kaoxin Pan[1,2], Qing Zhang[1,2*], Zhenyu Wang[1,2], Sibo Wang[2],
Aobo Zhou[2], Yong You[2], Decheng Wang[2]

(1. *Key Laboratory of Modern Agricultural Intelligent Equipment in South China, Ministry of Agriculture and Rural Affairs, Guangzhou 510630, China;*
2. *College of Engineering, China Agricultural University, Beijing 100083, China*)

Abstract: In response to the weaknesses of traditional agricultural equipment chassis with poor environmental adaptability and inferior mobility, a novel unmanned agricultural machinery chassis has been developed that can operate stably and efficiently under various complex terrain conditions. Initially, a new wheel-legged structure was designed by drawing inspiration from the motion principles of locust hind legs and combining them with pneumatic-hydraulic linkage mechanisms. Kinematic analysis was conducted on this wheel-legged configuration by utilizing the D-H parameter method, which revealed that its end effector has a travel range of 0-450 mm in the *X*-direction, 0-840 mm in the *Y*-direction, and 0-770 mm in the *Z*-direction, thereby providing the structural foundation for features such as independent four-wheel steering, adjustable wheel track, automatic vehicle body elevation adjustment, and maintaining a level body posture on different slopes. Subsequently, theoretical analysis and structural parameter calculations were completed to design each subsystem of the unmanned chassis. Further, kinematic analysis of the wheel-legged unmanned chassis was carried out using RecurDyn, which substantiated the feasibility of achieving functions like slope leveling and autonomous obstacle negotiation. An omnidirectional leveling control system was also established, taking into account factors such as pitch angle, roll angle, virtual leg deployment, and center of gravity height. Joint simulations using Adams and Matlab were performed on the wheel-legged unmanned chassis, comparing its leveling performance with that of a PID control system. The results indicated that the maximum absolute value of leveling error was 1.08° for the pitch angle and 1.19° for the roll angle, while the standard deviations were 0.216 47° for the pitch angle and 0.176 22° for the roll angle, demonstrating that the wheel-legged unmanned chassis surpassed the PID control system in leveling performance, thus validating the correctness and feasibility of its full-directional body posture leveling control in complex environments. Finally, the wheel-legged unmanned chassis was fabricated, assembled, and subjected to in-place leveling and ground clearance adjustment tests. The experimental outcomes showed that the vehicle was capable of achieving in-place leveling with response speed and leveling accuracy meeting practical operational requirements under the action of the posture control system. Moreover, the adjustable ground clearance proved sufficient to meet the demands of actual obstacle crossing scenarios.
Keywords: hilly areas, bionic machinery, wheel-legged vehicle, posture control, prototype testing
DOI: 10.25165/j.ijabe.20241705.8383

1 Introduction

The development of agricultural mechanization is crucial for promoting the modernization of agriculture[1]. However, the level of agricultural mechanization in China is not high, resulting in each agricultural worker being able to manage only 7.28-21.85 hm² of farmland, which falls far short of the 2428 hm² that can be managed by a laborer in developed Western countries[2]. This indicates an urgent need to enhance the level of agricultural modernization in China and develop a series of modern agricultural intelligent equipment to reduce labor costs and increase food production. Given the topographical characteristics of fewer plains and more hilly mountainous areas in China, many agricultural lands in various regions are dominated by terraced fields and sloping terrain[3], greatly increasing the difficulty of agricultural mechanized equipment operation. Most conventional agricultural mechanized equipment is suitable for working in flat areas and is not adapted to the varied terrain and steep slopes of hilly regions. Therefore, to meet the diverse agricultural operational needs in hilly and mountainous terrains, it is important to develop an intelligent unmanned chassis which has high obstacle-crossing capabilities and features all-directional leveling.

Wheel-legged vehicles combine the advantages of traditional wheeled vehicles and legged robots, possessing both the high mobility of wheeled vehicles and strong terrain adaptability and obstacle-crossing capabilities similar to legged robots[4]. In recent years, many researchers have conducted a series of studies on the

wheel-legged structure and posture control of wheel-legged vehicles[5-8]. Although a series of research achievements have been made, they have not been able to improve the driving stability of wheel-legged vehicles under complex road conditions[9-11]. Grand et al.[12] from France designed a series-connected wheel-legged robot called Hylos, consisting of four legs. Each leg is driven at its connection point by ball screw mechanisms and pneumatic actuators, with the end tires independently driven by DC motors. During operation, the robot can control the lifting and lowering movements of the four wheel legs separately based on terrain perception to achieve body leveling. Wang et al.[13,14] designed a wheel-legged robot using electric lift cylinders as wheel legs, where the extension of these cylinders directly affects parameters like wheelbase and body pitch angle. The body leveling function is achieved by independently driving the four electric cylinders, but this wheel-legged structure has poor obstacle-crossing performance. Wu et al.[15] designed a hydraulic-driven wheel-legged terrain vehicle with each leg having two degrees of freedom and two actuators. The reciprocating motion of the hydraulic cylinders in the upper and lower arms enables the swinging and extension of the wheel leg, ensuring stable movement in tripod and quadruped gaits as verified through combined simulations in Matlab and ADAMS. Bouton et al.[16] improved the motion characteristics of wheel-legged vehicles on irregular surfaces by altering wheel-legged drive components and employing obstacle detection technology. Vertical serial elastic drives connect the wheels to the chassis, adjusting the vertical forces acting on the wheels to ensure sufficient contact with the ground. Leveraging chassis inertia for obstacle traversal significantly enhances obstacle-crossing capabilities. In order to solve the problems of weak environmental adaptability and poor mobility of traditional agricultural equipment chassis, combining the performance advantages of existing wheel-legged vehicles[17-19], developing an unmanned agricultural equipment chassis which can operate stably and efficiently under different complex terrain conditions will make an important contribution to the development of agricultural modernization in China[20-22].

Based on the above research status, this study adopts a biomimetic mechanical design method to associate the principle of locust hind foot movement with the functional requirements of vehicle wheel-legged mechanisms, and combines the principle of pneumatic and pneumatic linkage mechanism to design a new type of wheel-legged combination mechanism, which has the ability of large range height expansion and remote position swing. The key system design and prototype trial production have been completed. Based on NSGA-II, an omnidirectional leveling pose control system for a biomimetic mechanical wheel-legged vehicle was constructed, and the algorithm simulation verification of the pose control system was completed through the ADAMS-Matlab joint simulation model of the wheel-legged vehicle. The experiments were conducted on omnidirectional leveling of the vehicle body posture and automatic adjustment of ground clearance, and the test results met the expected requirements.

2   Materials and methods

2.1   Vehicle design

2.1.1   Vehicle structure design

The wheel-legged unmanned chassis in hilly and mountainous terrain primarily consists of four parts: the wheel-leg mechanism, steering mechanism, body, and power system. The complete three-dimensional model of the vehicle is depicted in Figure 1. In the wheel-leg mechanism, the hydraulic cylinder serves as the main

driving component, enabling the adjustment of the vehicle's height by controlling its extension and retraction. The planetary gear steering mechanism located at the steering knuckle is another crucial driving element, which allows individual wheels of the wheel-legged unmanned chassis to swing from 0° to 90° left or right. The upper arm can oscillate within a range of 0° to 45°. By coordinating with an electric cylinder and wedge block, and it can be locked in positions at 0° and 45° angles, facilitating changes in the wheelbase and track width of the wheel-legged unmanned chassis.
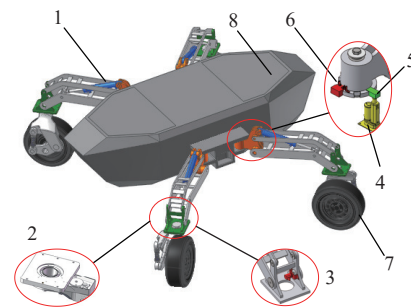
1. Hydraulic cylinder 2. Planetary gear steering mechanism 3. Steering knuckle 4. Cylinder 5. Wedge block 6. Angle sensor 7. Wheel assembly 8. Vehicle body

Figure 1   Diagram of wheel-legged unmanned chassis complete vehicle model

2.1.2   Hydraulic system design

The hydraulic cylinder is the primary driving component of the wheel-legged assembly. The vehicle's height adjustment can be achieved by controlling the extension and retraction of the hydraulic cylinder rod. It is essential to carry out parameter design for selecting an appropriately sized hydraulic cylinder product. Figure 2 illustrates the force analysis on the lever end of the hydraulic cylinder in the wheel-legged mechanism. F_A represents the thrust force applied by the hydraulic cylinder rod, while F_x and F_z denote the horizontal and vertical components of this force.
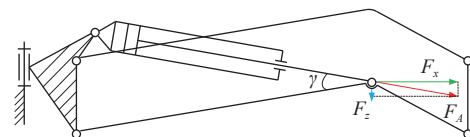
Figure 2   Force analysis of hydraulic cylinder

It is evident through the analysis that during the motion of the wheel-legged mechanism, the upper bracket and lower bracket are connected to the steering joint, which is directly linked to the wheels and their suspension components. One end of the upper and lower brackets of the four wheel legs is connected to the steering joint, providing support for the entire vehicle. The parameters of the hydraulic cylinder have been calculated using relevant formulas, and an existing double-acting hydraulic cylinder with a length that meets the design requirements has been selected.

2.1.3   Power system design

The wheel-legged unmanned chassis utilizes wheel hub motors to achieve four-wheel drive. Therefore, the parameter design of the wheel hub motor is crucial for determining whether the vehicle can achieve the expected power performance. As this vehicle model falls under agricultural off-road vehicles, acceleration performance of the entire vehicle is not considered. Power parameter calculations are focused solely on aspects like maximum speed and maximum climbing slope.

After calculating the maximum power and torque required for

the wheel hub motor using relevant formulas, a specific wheel hub motor has been selected. The performance parameters of this wheel hub motor are listed in Table 1.

Table 1   Wheel hub motor parameters

Parameters	Values
Rated power/kW	0.8
Peak power/kW	2
Rated power/r·min^{-1}	80
Peak power/r·min^{-1}	200
Rated torque/N·m	200
Peak torque/N·m	500
Voltage/V DC	48
Current/A	20

The selection of battery power should meet the power requirements of the vehicle during driving, and also ensure that the vehicle can provide acceleration or climbing power requirements even when the battery discharge reaches a certain depth. The parameter design of the wheel-legged unmanned chassis power battery can be calculated by Equation (1) for the instantaneous power of the vehicle operating at a constant speed of 10 km/h.

$$P_v = \frac{1}{3600\eta_T} \left(m \cdot g \cdot f + \frac{C_D \cdot A \cdot u_v^2}{21.15} \right) \cdot u_v \qquad (1)$$

a. Diagram of the chassis of the vehicle

where, P_v is the power required for constant speed driving, kW; η_T is the vehicle powertrain system efficiency; m is the full load mass, kg; g is the gravitational acceleration, m/s^2; f is the rolling resistance coefficient; C_D is the air resistance coefficient; A is the windward area, m^2; u_v is the constant speed, km/h.

The battery capacity was calculated as 3.57 kW·h based on running for 3 h. The standard box for lithium-ion power batteries was selected, with a total battery capacity of 11.32 kW·h. While meeting the driving range requirements, it can also provide power to other accessories on the vehicle.

2.1.4   Body structure design

The wheel-legged unmanned chassis employs a load-bearing body structure, with the chassis serving as its primary load-bearing component. The three-dimensional structural diagram of the chassis of the vehicle is depicted in Figure 3a. Hollow square tubes are chosen as the material for the chassis. Compared to round tubes and other solid materials, hollow square tubes offer a lighter weight while maintaining equivalent bending and torsional strength, which helps reduce the overall weight of the vehicle. Thin-walled panels are used to fill the gaps between adjacent square tubes of the chassis. These thin-walled panels primarily serve the purpose of encapsulating the body and act as non-load-bearing components. The encapsulated body's outer shape is illustrated in Figure 3b.

b. Diagram of theouter shape

Figure 3   Structure diagram of the body

2.2   Wheel-legged structure and working principle

2.2.1   Wheel-legged structure

The wheel-legged structure is a crucial component of the wheel-legged unmanned chassis, serving as a breakthrough point to achieve key technological goals such as autonomous obstacle crossing and posture leveling. The design of the wheel-legged structure is based on biomimetic principles, taking inspiration from multi-legged creatures in nature, particularly their leg characteristics used as a reference for the design of the wheel-legged structure. Locusts serve as a reference for the design of the wheel-legged structure of the unmanned chassis because of their well-developed hind legs and strong mobility. Figure 4a illustrates the construction of a locust's hind leg, which consists of segments including the basal, thigh, tibial, and foot ends, interconnected by joints. When the rear leg touches the ground, the contact between the tarsus and the ground is typically considered equivalent without delving into tarsal posture issues. Therefore, based on the structural characteristics of a locust's hind leg, the configuration of the wheel-legged structure of the wheel-legged unmanned chassis is depicted in Figure 4b.

To create a significant elevation difference between the start and end positions of the mechanism's motion, assisting the wheel-legged unmanned chassis in achieving body lifting and lowering actions, the pneumatic-hydraulic dynamic linkages can be effectively utilized in the wheel-legged structure of the unmanned chassis. The pneumatic-hydraulic dynamic linkage is a typical

group of rods with variable lengths, featuring a simple structure that is easily automated or semi-automated for control. Additionally, since the tires are mounted at the end of the leg structure, it is essential to enhance the overall structural strength of the wheel-legged components and ensure the stability of tire installation. For that, a parallel four-bar linkage mechanism is introduced based on the pneumatic-hydraulic dynamic linkage, forming the structure as shown in Figure 5. In the figure, the same letter with different subscripts represents the position of the same point at different times. Points A and D are fixed points and lie on the same vertical line. Rod AF is equal in length to rod DE, while the length of rod EF matches the distance between points A and D. Points A, F, E, and D are located at the four vertices of a parallelogram. As the actuator hydraulic cylinder BC extends, rod AF rotates around fixed point A, simultaneously driving rod EF. Rod EF then drives rod DE to rotate around fixed point D. Constrained by rods AF and DE, rod EF remains vertically downward, parallel to AD. When the tire is mounted on the axis where EF is located, the entire motion process ensures that the tire remains perpendicular to the ground. This design results in a stable straight-line driving capability and robust steering performance for the locomotion system.

The combination of the pneumatic-hydraulic dynamic linkage and the parallel four-bar linkage forms the wheel-legged structure, enabling the end of the wheel-legged mechanism to perform lifting and lowering movements within a certain range while maintaining the vertical orientation of the leg's end member. This design feature

ensures that the vehicle can achieve stable straight-line driving. To impart lateral swinging and adjust the wheelbase functionality to the vehicle, a redesign based on Figure 5 is carried out. The pivot points A, D, and C are integrated into the same component, named as the upper arm. At the center point O of the upper arm, an axis perpendicular to the pivot points A, D, and C is designed for rotational movement, forming the schematic diagram of the wheel-legged structure as shown in Figure 6.

a. Locust hindfoot structure

b. Wheel-legged configuration
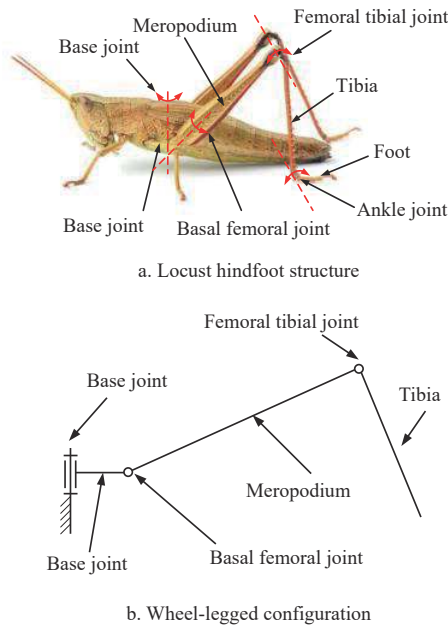
Figure 4   Application of bionics principle in wheel-legged mechanism
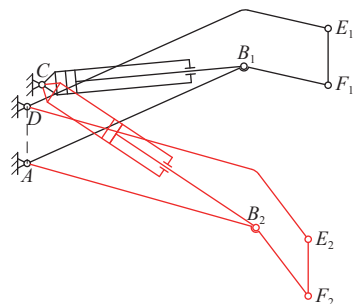
Figure 5   Pneumatic and pneumatic linkage combined with parallel four-link mechanism
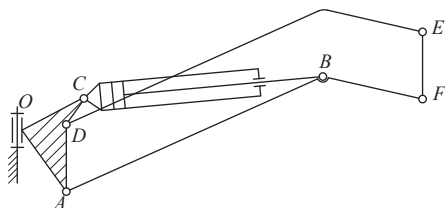
Figure 6   Schematic diagram of wheel-legged structure principle

After determining the structural form of the wheel-legged structure, in order to determine the number of active parts required for the wheel-legged mechanism, a degree of freedom analysis should be carried out to calculate the number of independent moving parts required to ensure the determined motion of the wheel-legged mechanism. The schematic diagram of the 7R1P mechanism of the wheel-legged mechanism is shown in Figure 7. P_5 in the figure represents the level of the motion, and the characters in parentheses represent the specific code of the motion pair, where R represents the rotating pair and P represents the moving pair.
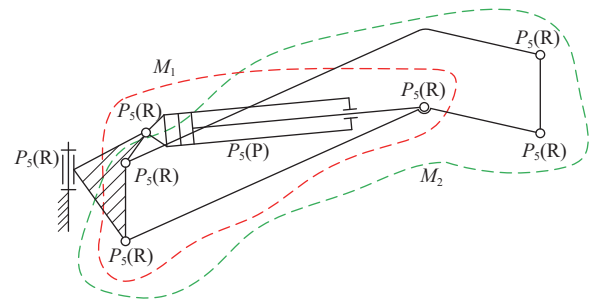
Figure 7   Schematic diagram of wheel-legged mechanism 7R1P

The wheel-legged mechanism 7R1P belongs to a multi-closed-loop spatial mechanism, and its degrees of freedom are calculated using Equation (2).

$$F = P_5 + 2P_4 + 3P_3 + 4P_2 + 5P_1 - \sum_{i=1}^{k}(6 - M_i)$$
$$k = \sum P - n = P_5 + P_4 + P_3 + P_2 + P_1 - n \tag{2}$$

where, F is the degree of freedom of the mechanism; P_1, P_2, P_3, P_4, and P_5 are the corresponding number of motion pairs at each level; k is the number of closed loops; M_i is the number of common constraints for the closed loop; n is the number of active components.

The wheel-legged mechanism 7R1P is composed of an upper arm, a hydraulic cylinder liner, a hydraulic cylinder rod, and three rods that form a parallel four-link mechanism, with n taken as 6. The motion pair consists of seven rotating pairs and one moving pair, all of which are level V, so P_5 is taken as 8, and P_1, P_2, P_3, and P_4 values are 0. The mechanism includes a closed loop M_1 formed by the lower links of the boom, hydraulic cylinder, and parallel four-link mechanism, and a closed loop M_2 formed by the three links of the boom and parallel four-link mechanism. Therefore, the k value of the two closed loops is taken as 2, and $M_1=M_2=3$. According to Equation (2), the degree of freedom F of the wheel-legged mechanism is 2, which indicates that the motion of two original parts must be determined, and the corresponding motion of the hydraulic cylinder and arm, i.e., the motion of the wheel-legged mechanism, is determined.

Based on the principle of the wheel-legged mechanism shown in Figure 6, three-dimensional design of the wheel-legged mechanism is carried out to form a three-dimensional model of the wheel-legged unmanned chassis leg structure shown in Figure 8. The leg structure consists of upper arm, upper support, lower support, steering knuckle, and hydraulic cylinder. Ribbed plates are distributed in the upper support, lower support, and steering knuckle to strengthen the overall structure of wheel and leg components.
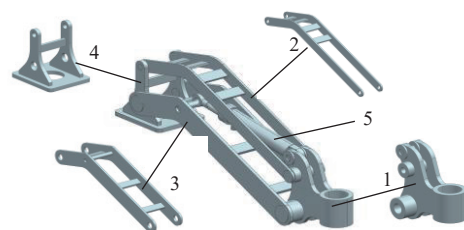
1. Upper arm 2. Upper support 3. Lower support 4. Knuckle 5. Hydraulic cylinder
Figure 8   Three-dimensional model of wheel-legged structure

2.2.2   Working principle

The kinematic analysis of the wheel-legged mechanism utilizes the Denavit-Hartenberg (D-H) parameter method to derive the pose matrix of the end point of the leg relative to the vehicle's center

coordinates. This process helps to establish the kinematic equations of the wheel-legged structure. Given that the four legs of the wheel-legged unmanned chassis are symmetrically arranged on the vehicle body and have identical structures, modeling and analysis are typically performed using the right front leg as a representative example. Due to the interconnected motion of the upper and lower links in the parallel four-bar linkage mechanism, the actual displacements are the same. Therefore, the upper link can be omitted during kinematic analysis, focusing primarily on the lower link. Eventually, the kinematic model of the right front leg is established as depicted in Figure 9.
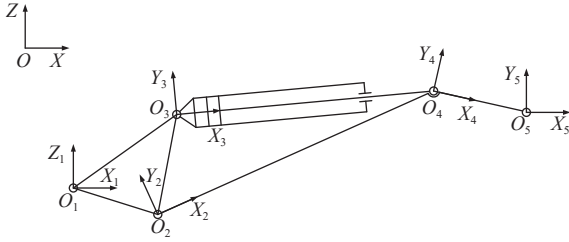
Figure 9   Kinematic model of right front leg

In Figure 9, the coordinate system $\sum OXYZ$ is the vehicle body center coordinate system. The X-axis is positively along the direction of travel of the vehicle, the Z-axis is vertically upward, and the Y-axis is perpendicular to the XOY plane. The coordinate system $\sum O_1X_1Y_1Z_1$ origin O_1 is the rotation center of the rotating pair R_1 connected with the body and the arm, and its initial coordinate axis direction is parallel to that of the body center coordinate system $\sum OXYZ$. The coordinate system $\sum O_2X_2Y_2Z_2$ origin O_2 is the rotating center of the rotating pair R_2 connected to the lower support and the upper arm. The coordinate system $\sum O_3X_3Y_3Z_3$ origin O_3 is the rotating center of the rotating pair R_3 connected by the hydraulic cylinder block and the upper arm. The coordinate system $\sum O_4X_4Y_4Z_4$ origin O_4 is the rotating center of the rotating pair R_4 connected by the push rod of the hydraulic cylinder and the lower support. Coordinate system $\sum O_5X_5Y_5Z_5$ origin O_5 is the rotation center of the rotating pair R_5 connected to the lower support and steering knuckle. Let the coordinates of the center point O_1 of the arm in the O coordinate system be (m, n, p), and remember that the rotation angle of the arm around the Z_1 axis is α; then the transformation matrix Equation (3) from the O coordinate system to O_1 is given.

$$ {}_0^1\boldsymbol{T} = \textbf{Trans}(x,m) \cdot \textbf{Trans}(y,n) \cdot \textbf{Trans}(z,p) \cdot \textbf{Rot}(z,\alpha) \qquad (3) $$

where, **Trans** represents transformation matrix; **Rot** represents rate of turning matrix.

Similarly, Equations (4)-(6) can be obtained.

$$ {}_1^3\boldsymbol{T} = \textbf{Rot}(x,\theta_{13}) \cdot \textbf{Rot}(z,\alpha_2) \cdot \textbf{Trans}(x,l_{13}) \cdot \textbf{Rot}(z,\alpha_{13}) \qquad (4) $$

$$ {}_3^4\boldsymbol{T} = \textbf{Trans}(x,l_{34}) \cdot \textbf{Rot}(z,\alpha_{34}) \qquad (5) $$

$$ {}_4^5\boldsymbol{T} = \textbf{Trans}(x,l_{45}) \cdot \textbf{Rot}(z,\alpha_{45}) \qquad (6) $$

The transformation matrix of coordinate system $\sum O_5$ to $\sum O$ is obtained.

$$ {}_0^5\boldsymbol{T} = {}_0^1\boldsymbol{T}{}_1^3\boldsymbol{T}{}_3^4\boldsymbol{T}{}_4^5\boldsymbol{T} = \begin{bmatrix} \boldsymbol{R}_0^5 & \boldsymbol{P}_0^5 \\ 0 & 1 \end{bmatrix} = \begin{bmatrix} a_{11} & a_{12} & a_{13} & p_x \\ a_{21} & a_{22} & a_{23} & p_y \\ a_{31} & a_{32} & a_{33} & p_z \\ 0 & 0 & 0 & 1 \end{bmatrix} \qquad (7) $$

where, $\boldsymbol{R}_0^5$ represents posture of coordinate system; $\sum O_5$ in

coordinate system $\sum O$; $\boldsymbol{P}_0^5$ represents vector coordinates of coordinate system $\sum O_5$ in coordinate system $\sum O$.

The workspace is a crucial kinematic parameter for a locomotion mechanism, as it determines the adaptability and obstacle-crossing capabilities of the vehicle with respect to the ground and external working environments. The shape and size of the workspace have a significant impact on the performance of the locomotion mechanism. The variation in the position of the center point O_5 at the end of the wheel-legged structure of the unmanned chassis can be calculated using Equation (8).

$$ \boldsymbol{P}_0^5 = \begin{bmatrix} p_x \\ p_y \\ p_z \end{bmatrix} = $$

$$ \begin{bmatrix} l_{45}\cos\alpha\cos(a_1+\alpha_{12}+\alpha_3)+l_{24}\cos\alpha\cos(\alpha_1+\alpha_{12})+l_{12}\cos\alpha\cos\alpha_1+m \\ l_{45}\sin\alpha\cos(a_1+\alpha_{12}+\alpha_3)+l_{24}\sin\alpha\cos(\alpha_1+\alpha_{12})+l_{12}\sin\alpha\cos\alpha_1+n \\ l_{45}\sin(\alpha_1+\alpha_{12}+\alpha_3)+l_{24}\sin(a_1+\alpha_{12})+l_{12}\sin\alpha_1+p \end{bmatrix} $$
$$ (8) $$

where, α is the arm rotation angle, (°); l_{34} is the cylinder length, mm.

Those determine constants were obtained based on design structure, l_{12}=220 mm, l_{13}=315 mm, l_{23}=254 mm, l_{24}=750 mm, l_{45}=272 mm, α_1=17°, α_2=36°, α_3=36.9°, $\angle O_1O_2O_3$=83.1°, $\angle O_1O_3O_2$=43.8°, $\angle O_2O_4O_5$=143°, and the angle between O_2O_3 and horizontal X-axis is 79.8°. The process variable α_{12} is obtained from cosine theorem.

The theoretical expression for the variation in the position of the center point O_5 at the end of the wheel-legged structure of the unmanned chassis shows that the X and Y coordinates of the center point O_5 are influenced by the rotation angle of the upper arm around the Z_1 axis and the length l_{34} of the hydraulic cylinder. On the other hand, the Z-axis coordinate of the center point O_5 is independent of the rotation angle of the upper arm around the Z_1 axis but is related to the angle α_{12}, which is in turn affected by the length l_{34} of the hydraulic cylinder. Thus the Z-axis position coordinate of the center point O_5 is solely influenced by the length l_{34} of the hydraulic cylinder. Based on this information, Equation (8) can be abbreviated to Equation (9).

$$ \boldsymbol{P}_0^5(p_x,p_y,p_z)=f(\alpha,l_{34}) \qquad (9) $$

In Figure 9, $\angle O_2O_4O_3$ represents the transmission angle of the wheel-legged mechanism, reflecting its transmission performance. The relationship curve between the transmission angle of the wheel-legged mechanism and the length variation of the hydraulic cylinder is illustrated in Figure 10. Throughout the entire motion process, there are no points where the transmission angle equals 0, indicating the absence of dead points within this range of motion for the wheel-legged structure. In theory, as long as the force provided by the hydraulic cylinder meets the requirements, the wheel-legged mechanism can achieve its intended motion without encountering any dead spots.

From Equation (8) of the change of the position of the center point O_5 at the end of the wheel-legged mechanism, it can be seen that the position coordinates of the X and Y axes of the center point O_5 at the end of the wheel-legged mechanism are affected by the rotation angle α of the arm around the Z_1 axle and the length of the hydraulic cylinder l_{34}. The Z-axis position coordinate of the center point O_5 at the end of the wheel-legged mechanism is independent of the angle at which the arm rotates around the Z_1 axis and is related to the angle α_{12}, while the angle α_{12} is affected by the length

of the hydraulic cylinder l_{34}, i.e., the Z-axis position coordinate of the center point O_5 at the end of the wheel-legged mechanism is only affected by the length of the hydraulic cylinder l_{34}. By substituting α_{12} and other known parameters, the expression of the change of the position of the center point O_5 at the end of the wheel-legged mechanism with unmanned chassis is obtained, where p_x, p_y are functions determined by α and l_{34}, and p_z is a function determined only by l_{34}.

The Matlab plotting function is used to plot the track points of p_x, p_y, and p_z, where m, n, and p are all 0, in order to study the displacement of the end of the wheel leg relative to the center of the arm. When plotting the locus points of p_x and p_y, l34 takes the value [640,840], while α starts from 0° and increases incrementally in value by 5° until reaching 45°. When plotting the trace points of p_z, l_{34} takes the value [640,840]. Subsequently, the drawing is redrawn in Origin and the drawing details are optimized. Figure 11 shows the motion space of the right front leg end in the XOY, XOZ, and YOZ planes respectively. It can be seen that the working range in X direction is 750-1200 mm, in Y direction is 0-800 mm, and in Z direction is –600-200 mm.

Based on the variations in the length l_{34} of the hydraulic cylinder and the swing angle of the upper arm, a geometric method is employed to plot the workspace of the right front leg end. By

following this approach, the workspace diagram of the right front leg end is obtained, as shown in Figure 12. From Figure 12a, it is evident that the trajectory surface at the end of the wheel-legged mechanism is a smoothly transitioning curve, indicating gentle undulations of the vehicle body throughout the entire process. Furthermore, Figure 12b illustrates that the wheel-legged mechanism has a large workspace, implying excellent operational capabilities.
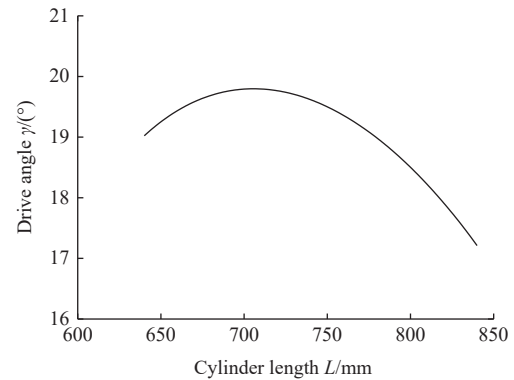
Figure 10   Variation curve of driving angle of wheel-legged mechanism

a. In *XOY* plane   b. In *XOZ* plane   c. In *YOZ* plane
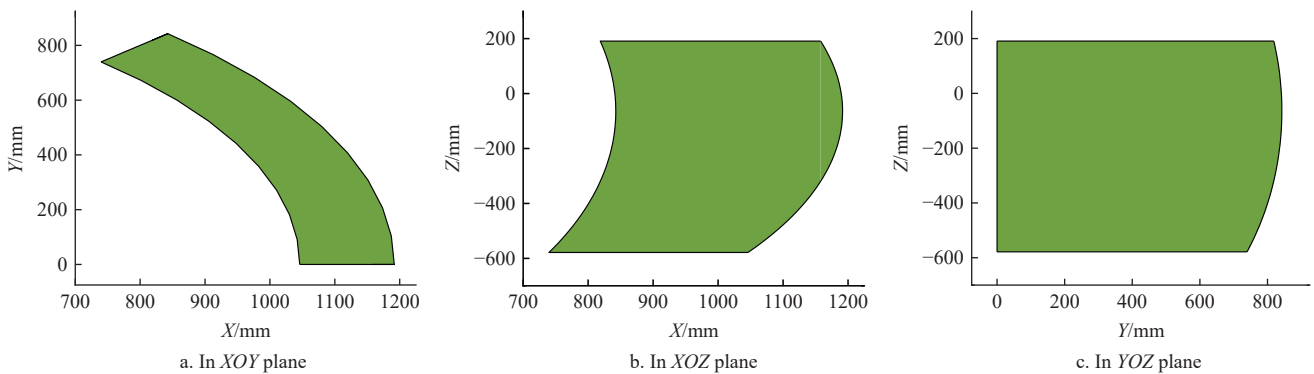
Figure 11   Movement space of right front leg end
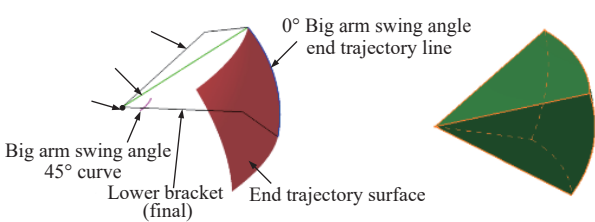
Figure 12   Right front leg workspace

3   Results and discussion

3.1   Simulation analysis of kinematics and pose control

3.1.1   Simulation model construction

1) Rigid body model

Before establishing a multi-body dynamics model, the three-dimensional model of the wheel-legged unmanned chassis was simplified to reduce unnecessary constraints during assembly and enhance modeling flexibility. The simplified model is depicted in Figure 13. In addition, it is essential for components in the dynamic model to possess mass properties. In RecurDyn, material properties are assigned to components, and the software automatically calculates the mass of each component based on its volume. In this study, the mass of the wheel-legged components is set as aluminum. The mass of components such as the chassis, wheel hub drive

system assembly, and heavy items is manually assigned through custom values. After assignment, the distribution of mass for each component is detailed in Table 2.
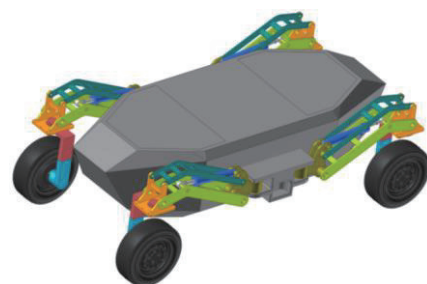
Figure 13   Rigid body model of wheel-legged unmanned chassis

2) Simulated road surface

In the process of kinematics simulation, except for the kinematics simulation analysis of a single wheel leg, the simulation of other working conditions needs to create a road surface as the support surface of the tire, and provide the ground friction effect when traveling. For different simulation conditions, the required road geometry also varies. Figure 14 shows different road surface models under various simulation conditions.

As all four wheel-legged structures are identical and

symmetrically distributed on the vehicle body, constraints are added to each component using the example of the front right leg. The constraint relationships for the kinematic simulation model of the front right leg are configured as shown in Figure 15. The diagram excludes the ground, vehicle body, heavy items, and the other three wheel legs. The contact between the tire and the ground surface, denoted as SolidContact1, is not indicated in the figure.

Table 2   Mass of each component of the model

Component Name	Mass/kg	Quantity	Total/kg
Body	528	1	
Big arm	19	4	
Upper support	5.5	4	
Lower support	15	4	
Hydraulic cylinder barrel	6.5	4	
Hydraulic cylinder rod	4.5	4	1546
Knuckle	9	4	
Steering bend	12	4	
Tire connection plate	12	4	
Tire (including hub motor)	46	4	
Heavy objects	500	1	

a. The ramp road surface was created specifically for simulation of climbing conditions

b. Vertical obstacle road surface is used for simulation verification of vertical obstacle crossing
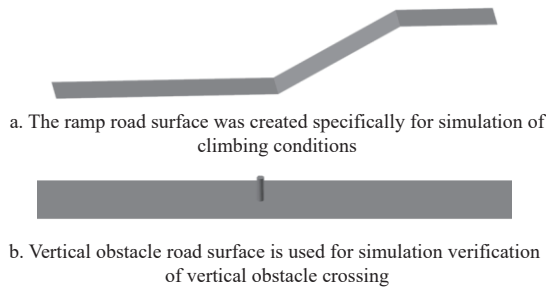
Figure 14   Different road surface models under different simulation conditions
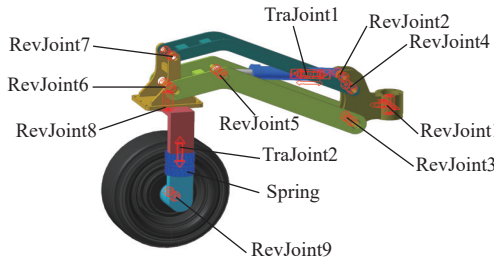
Figure 15   Constraint relationships in the simulation model

3.2   Kinematics simulation analysis

3.2.1   Vehicle body leveling on different slopes

The length of the hydraulic cylinder is the sole variable that impacts the change in the vehicle's center of mass. Understanding the relationship between the length of the hydraulic cylinder and the tilt angle of the vehicle is fundamental for achieving controllable leveling functionality. For different sloped surfaces, such as slopes and side slopes, research has been conducted on the influence of hydraulic cylinder length variation on the change in the vehicle's tilt angle. In this study, the maximum stroke of the hydraulic cylinder is set at 200 mm. The driving information added to each actuator is detailed in Table 3.

Figure 16 shows a schematic diagram of the leveling of the vehicle body when driving on a sloping road using a wheel-legged unmanned chassis. Figure 16a shows the initial posture of the vehicle on a sloping road surface. It can be seen that the body remains parallel to the slope, and it is necessary to drive the rear hydraulic cylinder to extend and lift the rear of the vehicle to

achieve the body leveling shown in Figure 16b. In the simulation process of sloping road surfaces, the rear hydraulic cylinder is the driving cylinder, and the front hydraulic cylinder is the non-driving cylinder.

Table 3   Kinematic pair drive information

Constraint name	Type		Driving function
RevJoint1	Displacement (time)		0
RevJoint8	Displacement (time)		0
RevJoint9	Speed (time)		0
TraJoint1	Displacement (time)	Driving cylinder	STEP (time,0,0,3,200)
		Non-driving cylinder	0

a. Initial posture   b. Body leveling
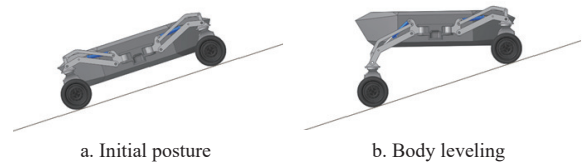
Figure 16   Schematic diagram of vehicle body leveling when driving on sloping roads

In the post-processing analysis module, the data of vehicle inclination and drive cylinder displacement are exported, and the variation curve between the vehicle leveling angle and hydraulic cylinder displacement is obtained, as shown in Figure 17. From the figure, it can be seen that the two are approximately linearly related. On a sloping road, the maximum adjustable inclination of the vehicle is about 16°, which means that the wheel-legged unmanned chassis can maintain the horizontal state of the vehicle body by driving the hydraulic cylinder on slopes within the range of 0°-16°.
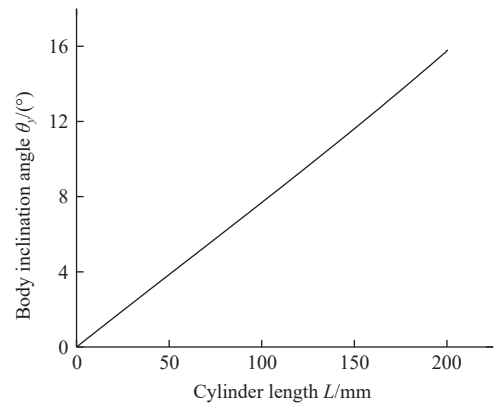
Figure 17   Curve of vehicle leveling angle change on sloping road surface

Figure 18 shows a schematic diagram of the leveling of the vehicle body while driving on a side slope with a wheel-legged unmanned chassis. Figure 18a shows the initial posture of the vehicle on a sloping road surface, indicating that it is necessary to drive the hydraulic cylinder of the side wheel legs below the slope to achieve the vehicle body leveling shown in Figure 18b. In the side slope road surface simulation process, the hydraulic cylinder of the lower side leg on the slope is the driving cylinder, and the hydraulic cylinder of the upper side wheel leg on the slope is the non-driving cylinder.

In the post-processing analysis module, the data of vehicle inclination and displacement of the driving cylinder are exported, and the variation curve between the leveling angle of the vehicle and the displacement of the hydraulic cylinder is obtained as shown in Figure 19, which is similar to the linear relationship between the

results of the slope road. On the slope road, the maximum adjustable inclination of the vehicle is about 27°, which means that the wheel-legged unmanned chassis can maintain the horizontal state of the vehicle body by driving the hydraulic cylinder on the slope within the range of 0° to 27°.

a. Initial posture   b. Body leveling
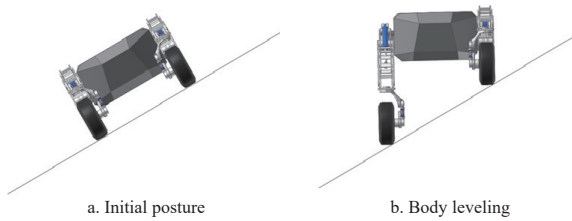
Figure 18   Schematic diagram of vehicle body leveling when driving on side slopes
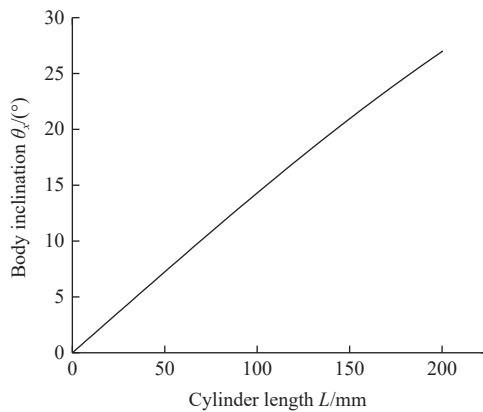
Figure 19   Curve of vehicle leveling angle change on side slope road surface

3.2.2   Vertical obstacle crossing

The change in the center of mass height of the wheel-legged unmanned chassis is solely influenced by variations in the length of the hydraulic cylinder. During the vertical obstacle crossing simulation, it is necessary to set appropriate driving functions for RevJoint9 and TraJoint1 to respectively drive the motion of the hydraulic cylinder and the rotation of the wheels. As for the kinematic pairs RevJoint1 and RevJoint8, their driving functions should be set to 0 to restrict the motion of the connected components. The driving information for the vertical obstacle crossing simulation is listed in Table 4.

Table 4   Kinematic pair drive information

Constraint name	Type	Driving function
RevJoint1	Displacement (time)	0
RevJoint8	Displacement (time)	0
RevJoint9	Speed (time)	STEP (time,0,0,4,21)
TraJoint1	Displacement (time)	STEP (time,5,0,6,STEP (time, 6,200,7,STEP (time,7,200,8,0)))

Figure 20 illustrates the vertical obstacle crossing simulation process of the wheel-legged unmanned chassis. Before encountering the obstacle, as shown in Figure 20a, the vehicle maintains normal driving with a certain ground clearance. When facing the obstacle, as depicted in Figure 20b, the hydraulic cylinder is actuated to lift the vehicle, resulting in a larger ground clearance that enables the vehicle to smoothly overcome the obstacle. After clearing the obstacle, as shown in Figure 20c, the hydraulic cylinder retracts, lowering the center of mass of the vehicle and returning it to a normal driving state.

The post-processing module derives the relevant data of the

change of the body center of mass of the wheel-legged unmanned chassis over time, and then processes the data according to the distance from the body center of mass to the bottom surface of the body to obtain the relevant data of the change of the wheel-legged unmanned chassis ground clearance over time. Figure 21 shows the change curve of vehicle ground clearance in the process of vertical obstacle crossing simulation. Combined with the driving function set by the figure and the hydraulic cylinder, it can be seen that when the hydraulic cylinder is extended by 200 mm, the vehicle ground clearance is more than 800 mm, which indicates that the wheel-legged unmanned chassis meets the functional requirements of vertical obstacle crossing.

a. Before obstacle crossing

b. In the process of obstacle crossing

c. After obstacle crossing
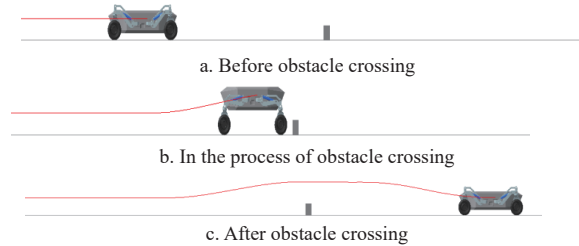
Figure 20   Schematic diagram of vertical obstacle clearance
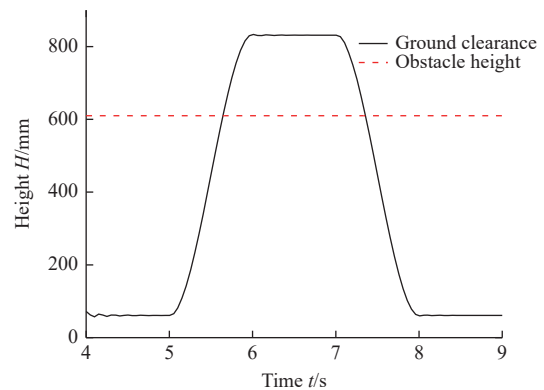
Figure 21   Curve of vehicle ground clearance variation during vertical obstacle crossing simulation

3.3   Simulation and analysis of pose control

3.3.1   Kinematic model

From the kinematics analysis of the wheel-legged mechanism, the mathematical relationship between the position coordinate wi of the end point of the wheel leg in the body center coordinate system, the hydraulic cylinder length L_i, and the swing angle α of the wheel leg boom is derived. Equation (10) is the relative position function of the wheel center.

$$w_i = \boldsymbol{P}_0^5(p_x, p_y, p_z)_i = f_i(L_i, \alpha_i) \tag{10}$$

The rotation matrix $\boldsymbol{R}$ is obtained from the three attitude parameters R, P, Y of the roll, pitch, and yaw of the car body, and the displacement matrix $\boldsymbol{T}_3$ is obtained from the position coordinates (x, y, z) of the origin of the car body coordinate system under the geodetic coordinate system. Finally, the pose transformation matrix $\boldsymbol{T}_2$ from the car body coordinate system to the geodetic coordinate system is derived.

$$R = \mathbf{Rot}(R) \cdot \mathbf{Rot}(P) \cdot \mathbf{Rot}(Y) =$$

$$\begin{bmatrix} 1 & 0 & 0 \\ 0 & \cos R & -\sin R \\ 0 & \sin R & \cos R \end{bmatrix} \begin{bmatrix} \cos P & 0 & -\sin P \\ 0 & 1 & 0 \\ \sin P & 0 & \cos P \end{bmatrix} \begin{bmatrix} \cos Y & -\sin Y & 0 \\ \sin Y & \cos Y & 0 \\ 0 & 0 & 1 \end{bmatrix} \tag{11}$$

$$T_3 = \begin{bmatrix} x \\ y \\ z \end{bmatrix} \qquad (12)$$

$$T_2 = \begin{bmatrix} R & T_3 \\ 0 & 1 \end{bmatrix} \qquad (13)$$

From this, the coordinates of the wheel center W_i in the geodetic coordinate system can be obtained through Equation (13).

$$W_i = T_2 \cdot w_i \qquad (14)$$

By substituting Equation (10) into Equation (14), the mathematical relationship Equation (15) between the coordinates of the wheel center in the geodetic coordinate system and the expansion and contraction of the wheel leg oil cylinder and the swing angle of the boom can be obtained, which is the absolute position function F_i of the wheel center. The input is the expansion and contraction of the wheel leg oil cylinder, roll angle, pitch angle, and yaw angle, as well as the position coordinates of the origin of the vehicle coordinate system in the geodetic coordinate system; the position coordinates of the wheel center in the geodetic coordinate system are the output.

$$W_i = F_i(L_1, L_2, L_3, L_4, R, P, Y, x, y, z) \qquad (15)$$

Based on the position coordinates of the wheel center in the geodetic coordinate system and the position coordinates of the wheel center in the vehicle coordinate system, the transformation matrix between the two coordinate systems can be derived. Two world coordinate systems of the same scale can be transformed through rotation and translation. To calculate the transformation relationship, it is necessary to know the coordinates of N corresponding points on both sides, which are set to A and B, then $B = R \cdot A + T$ can be solved. Due to the possibility of N being relatively large, this equation is usually overdetermined and can be calculated using Singular Value Decomposition (SVD), with the internal principle being the least squares method.

$$H = \sum_{i=1}^{N} \left(P_A^i - \text{centroid}_A \right) \left(P_B^i - \text{centroid}_B \right)^{\mathrm{T}} \qquad (16)$$

$$[U, S, V] = \text{SVD}(H) \qquad (17)$$

$$R = VU^{\mathrm{T}} \qquad (18)$$

$$T = -R\,\text{centroid}_A + \text{centroid}_B \qquad (19)$$

where, centroid_A is average center of A; centroid_B is average center of B.

The rotation matrix is calculated as Equation (20), and the roll angle, pitch angle, and yaw angle are calculated as Equations (21)-(23).

$$R = \begin{bmatrix} R_{11} & R_{12} & R_{13} \\ R_{21} & R_{22} & R_{23} \\ R_{31} & R_{32} & R_{33} \end{bmatrix} \qquad (20)$$

$$\text{roll} = \arctan(R_{32}/R_{33}) \qquad (21)$$

$$\text{pitch} = \arctan\left(-R_{31}/\sqrt{R_{32}^2 + R_{33}^2}\right) \qquad (22)$$

$$\text{yaw} = \arctan(R_{21}/R_{11}) \qquad (23)$$

Substituting Equation (10) into it can obtain the mathematical relationship between the spatial attitude parameters pitch, roll, and yaw angles, as well as the control parameters of the cylinder expansion and contraction, namely the spatial attitude function G. The mathematical relationship shown in Equation (24) is obtained by taking the expansion and contraction of the wheel-leg cylinder, and the position coordinates of the wheel center in the geodetic coordinate system as input; and the spatial attitude parameters pitch, roll, and yaw as output.

$$[R, P, Y] = G(L_1, L_2, L_3, L_4, W_1, W_2, W_3, W_4) \qquad (24)$$

3.3.2 NSGA-II algorithm control principle

The active attitude control of the vehicle in the process of obstacle crossing needs to comprehensively consider such factors as pitch angle, roll angle, weak leg, height of center of mass, etc.; design the control system; and adjust the expansion and contraction of the four wheel legs, as shown in Figure 22. When the vehicle crosses obstacles, the spatial attitude parameters are obtained through the inclination sensor installed on it, and the coordinates of each wheel center position are obtained according to Equation (24). A leveling control algorithm was designed based on the NSGA-II algorithm, with spatial attitude parameters, current wheel leg extension and extension, grounding force as input, and target attitude parameters as output, to achieve real-time control of the vehicle's spatial attitude during obstacle crossing.
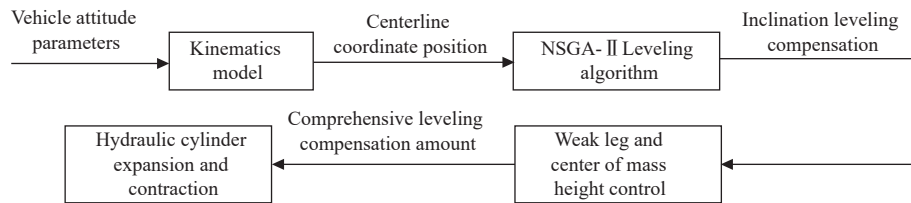
Figure 22   Control block diagram of omnidirectional leveling system

Tilt angle leveling requires consideration of pitch angle and roll angle. The NSGA-II algorithm can be used to solve such multi-objective optimization control problems. The leveling algorithm block diagram is shown in Figure 23, where parameters such as population boundary rules and iteration times are determined through simulation experiments. The objective function is the vehicle attitude angle determined by the expansion and contraction of each wheel leg in the population at the current absolute position of the wheel center. Then, through rapid non-dominated sorting and continuous iterative optimization operations such as calculating crowding distance, the corresponding wheel leg expansion and contraction amount within the population boundary that can maintain the minimum inclination angle of the vehicle at the current absolute position of the wheel center is obtained.

The coordinates of the wheel center in the geodetic coordinate system remain unchanged before and after the leveling action of the vehicle, so the absolute position coordinates of the wheel center are taken as the input, the current wheel leg expansion and contraction

amount is obtained through the vehicle inverse kinematics model, and then the initial population is generated. The population boundary rules here are shown in Equation (25).

$$[L_{iMIN}, L_{iMAX}] = [L_i - 2(R + P), L_i + 2(R + P)] \qquad (25)$$

After determining the compensation amount for tilt angle leveling, if the "weak leg" compensation is not carried out, there may be a suspended state of the wheel legs, reducing the driving force and even creating the risk of sudden tipping. The "weak leg" compensation control is based on the grounding force information obtained from the pressure sensor. When the grounding force is less than 100 N and lasts for 0.5 s, it is determined that the wheel legs are in the "weak leg" or suspended state, and the wheel leg

extension compensation is carried out. The judgment conditions are determined through simulation experiments.

After multiple inclination adjustments, there may be situations where the center of mass is too high, which not only increases the risk of tipping but also limits the subsequent leveling effect. Therefore, it is necessary to add center of mass height control to monitor the control parameter of attitude adjustment. When the four wheel legs maintain a certain extension exceeding 120 mm and remain unchanged for 0.75 s, it is determined that the vehicle is in a stable running state and no leveling action has been taken. The four wheel legs contract simultaneously to reduce the height of the vehicle's center of mass, and the judgment conditions are determined through simulation experiments.
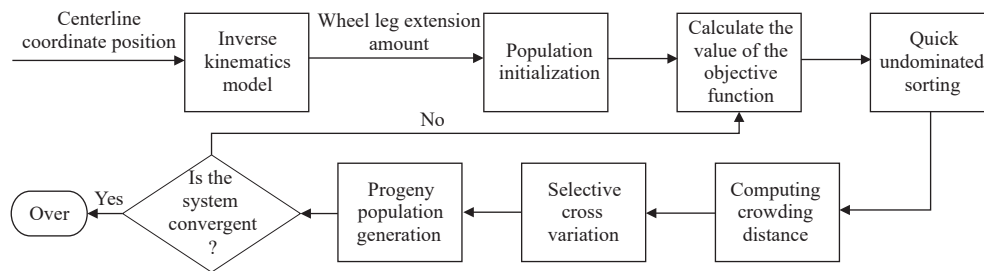
Figure 23   Diagram of NSGA-II leveling algorithm

3.4   Comparison of NSGA-II and PID control simulation effects

The model of wheel-legged unmanned chassis and obstacle road surface is established in ADAMS, kinematics simulation is carried out with Matlab/Simulink, and the PID control system is designed to compare with the omnidirectional leveling control system. The terrain that may be encountered in hilly and mountainous areas is simulated using the road surface model shown in Figure 24. The curved protrusion section is 10 m long and 1.3 m high, the first trapezoidal section is 10 m long and 0.3 m high with a slope of 15°, the second trapezoidal section is 9.5 m long and 0.5 m high with a slope of 30°, and the curved depression section is 7.2 m long and 0.4 m deep.

After the control model is built, simulation is conducted. The leveling control effect of the vehicle's pitch angle and roll angle is

shown in Figure 25. Compared with the PID control scheme, the PID control scheme has good control effect in the pitch direction compared to the omnidirectional leveling control scheme proposed in this paper. However, this scheme has higher leveling accuracy and speed. In the roll direction, this scheme adds weak leg compensation and centroid height control, reduces roll risk, and has significant advantages over PID control schemes. The maximum value of leveling error in this plan is pitch angle 1.08°, roll angle 1.19°, pitch angle standard deviation 0.216 47, and roll angle standard deviation 0.176 22.

Figure 24   Road model

a. Pitch angle variation curve

b. Roll angle variation curve
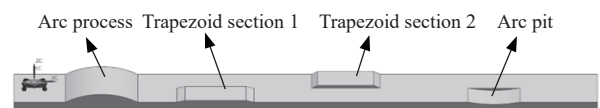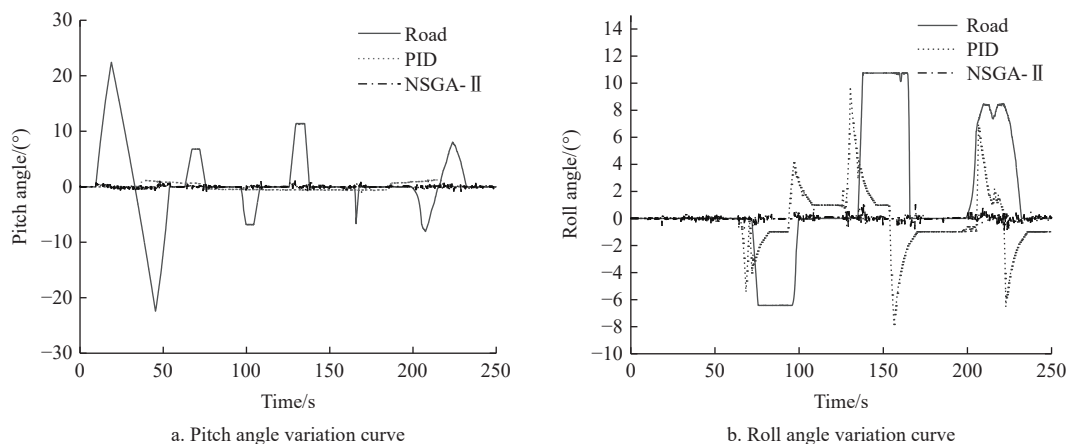
Figure 25   Comparison of leveling effects

3.5   Prototype trial production and testing

3.5.1   Prototype trial production

The wheel legs and body structure of the wheel-legged unmanned chassis are non-standard components that require customized processing. After parameter matching of components

such as power batteries, wheel hub motors, and hydraulic pump stations, mature products already available in the market are selected for purchase. After all the components are complete, the trial production of the wheel-legged unmanned chassis prototype is carried out. The actual prototype is shown in Figure 26.

Figure 26   Prototype physical object

3.5.2   Prototype testing

1) In-situ leveling test

The wheel-legged unmanned chassis should have an omnidirectional leveling ability, which means that the expansion and contraction of each hydraulic cylinder can be adjusted to ensure that the vehicle body is always in a horizontal position when the vehicle body tilts. This is of great significance for the stability of agricultural equipment operations. Therefore, the leveling ability of the wheel-legged unmanned chassis is verified through in-situ leveling tests of the prototype. The leveling process is shown in Figure 27. Firstly, a portion of the wheel legs are controlled to retract and retract, causing a certain range of inclination changes in the body. Then, the leveling switch is turned on, and the wheel-legged vehicle automatically performs leveling under the control of the vehicle controller. The angles before and after leveling and the leveling time are recorded. A total of 5 tests are conducted, and the results are summarized as listed in Table 5.

According to the data in the table, the average angle after leveling is about 0.8° pitch angle, 1.0° roll angle, and the average leveling time is about 1.2 s, which can meet the accuracy requirements during operation.

a. Before leveling
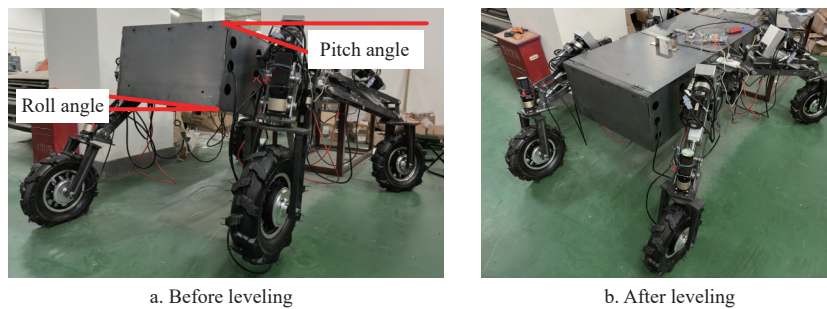
b. After leveling

Figure 27   In-situ leveling test

Table 5   In-situ leveling test data

No.	Angle before leveling		Angle after leveling		Leveling time/s
	Pitch angle/(°)	Roll angle/(°)	Pitch angle/(°)	Roll angle/(°)	
1	15.7	−2.2	−0.7	1.2	1.3
2	3.2	9.6	0.8	1.5	0.8
3	−10.9	10.1	−1.3	0.9	1.0
4	−15.1	3.2	1.1	−0.7	1.4
5	−7.9	−8.5	−0.2	0.5	1.6

2) Ground clearance adjustment test

The adjustment range of the ground clearance of the wheel-legged unmanned chassis corresponds to its obstacle clearance ability. It is verified whether the obstacle clearance ability meets the requirements by measuring its ground clearance under different hydraulic cylinder strokes. As shown in Figure 28, through controlling the hydraulic cylinder for expansion and contraction, then recording the ground clearance at the four corners of the body, the ground clearance change data are obtained and listed in Table 6. From the table, it can be seen that within the range of hydraulic cylinder travel, the ground clearance can vary between 24 mm and 574 mm, and the obstacle clearance height exceeds 500 mm, which can meet the actual obstacle clearance height requirements for field work.

a. Initial state

b. Ascending process

c. Maximum ground clearance
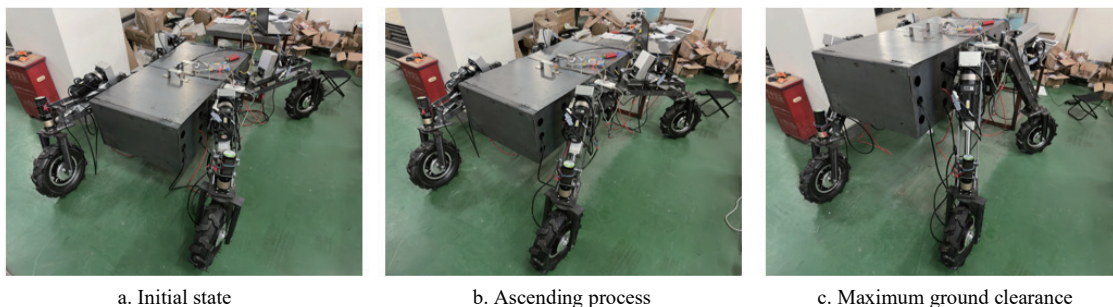
Figure 28   Ground clearance adjustment test

Table 6   Ground clearance adjustment test data

Hydraulic cylinder elongation/mm	Ground clearance/mm			
	Right front	Left front	Left rear	Right rear
0	24.5	25.1	24.7	24.2
30	134.6	135.3	134.2	134.7
60	244.2	244.6	244.2	244.0
90	354.0	354.1	354.0	354.2
120	464.7	464.6	464.0	464.0
150	574.3	574.3	574.5	574.1

4   Conclusions

The present study proposes a biomimetic mechanical wheel-legged vehicle configuration suitable for special terrain in hilly and mountainous areas, in response to the problems of low efficiency and poor stability of traditional agricultural machinery equipment when operating in hilly and mountainous areas. The conclusions can be drawn as follows.

1) By mimicking the movement principles of a locust's hind leg and incorporating a pneumatic-hydraulic continuous rod

mechanism, a new type of wheel-legged combined structure has been designed. The D-H parameter method was utilized to conduct kinematic analysis on this wheel-legged structure. The study verified that the end of this wheel-legged structure can move within the ranges of 0-450 mm in the X direction, 0-840 mm in the Y direction, and 0-770 mm in the Z direction. This provides a structural foundation for achieving various functions of the entire vehicle.

2) Based on the NSGA-II algorithm, an omnidirectional leveling pose control system for the biomimetic mechanical wheel-legged vehicle was constructed. The algorithm was verified through the ADAMS-Matlab joint simulation model of the wheel-legged vehicle. The results showed that the maximum pitch angle leveling error of the wheel-legged vehicle in complex hilly and mountainous terrain was 1.08°, the maximum roll angle leveling error was 1.19°, and the leveling effect was better than the traditional PID control algorithm.

3) Experiments were conducted with respect to omnidirectional leveling of vehicle posture and automatic adjustment of ground clearance. The results showed that the test prototype can achieve omnidirectional automatic leveling of vehicle posture in complex terrain, with an average leveling time of about 1.2 s and an average leveling error of 0.8°. The response speed and leveling accuracy of posture control can meet the actual working requirements of the vehicle. The ground clearance of the vehicle can be automatically adjusted within the range of 24-574 mm, which can meet the requirements of vehicles in the complex terrain of hills and mountains.

Acknowledgements

[References]

[1] Luo X W. Reflections on the development of agricultural mechanization in hilly and mountainous areas. Agricultural Machinery Technology Promotion, 2011; 2: 17–20. (in Chinese)

[2] Luo X W, Liao J, Zang Y, Qu Y G, Wang P. The development direction of agricultural production in China: from mechanization to intelligence. China Engineering Science, 2022; 24(1): 46–54. (in Chinese)

[3] Yang Z H. The current situation, problems and countermeasures of agricultural mechanization in hilly and mountainous areas. Southern Agricultural Machinery, 2022; 53(20): 72–74. (in Chinese)

[4] Zhai J H, Wang Y Q, Wei X H. Design and simulation of a search and rescue robot based on a wheel-leg detection vehicle structure. Mechanical Transmission, 2022; 46(2): 48–54. (in Chinese)

[5] Wang Y Q. Design and research of a search and rescue robot based on a wheel-leg swing arm suspension structure. Master dissertation. Fuxin:

[6] Ning M, Xue B L, Ma Z F. Design, analysis, and experiment for rescue robot with wheel-legged structure. Mathematical Problems in Engineering: Theory, Methods and Applications, 2017; 5: 1–16.

[7] Yan H. Research on composite wheel-leg robots for special forestry needs. Master dissertation. Beijing: Beijing Forestry University, 2019; 80p. (in Chinese)

[8] Sun Z B, Zhang D, Li Z L, Yan S, Wang N. Optimum design and trafficability analysis for an articulated wheel-legged forestry chassis. J. Mech. Des, 2022; 144(1): 013301.

[9] Li Z L, Liu J H, Sun Z B, Yu C Z. Dynamic research and analysis for a wheel-legged harvester chassis during tilting process. Advances in Mechanical Engineering, 2019; 11(6): 1687814019855453.

[10] Wang X W, Yuan S Q, Jia W D. Current situation and development of agricultural mechanization in hilly and mountainous areas. Journal of Drainage and Irrigation Machinery Engineering, 2022; 40(5): 535–540. (in Chinese)

[11] Brian H. Athlete: A Mobility and Manipulation System for the Moon. 2007 IEEE Aerospace Conference, 2007; 6(9): 3086–3095.

[12] Grand C, Benamar F, Plumet F. Motion kinematics analysis of wheeled–legged rover over 3D surface with posture adaptation. Mechanism and Machine Theory, 2009; 45(3): 477–495.

[13] Wang X W, Wang S K, Wang J Z. Electric parallel six wheeled legged robot based on a heteromorphic Stewart platform. Journal of Mechanical Transmission, 2020; 56(13): 84–92. (in Chinese)

[14] Kang X, Wang S K, Wang J Z. High-adaption locomotion with stable robot body for planetary exploration robot carrying potential instruments on unstructured terrain. Chinese Journal of Aeronautics, 2021; 34(5): 652–665.

[15] Wu D, Xu X, Sun C, Jiang Y. Planning research on leg movement of a wheel terrain vehicle. IEEE International Conference on Electrical Engineering and Mechatronics Technology (ICEEMT). IEEE, 2021; pp.60-65. doi: 10.1109/ICEEMT52412.2021.9601860.

[16] Bouton A, Grand C, Benamar F. Motion control of a compliant wheel-leg robot for rough terrain crossing. IEEE International Conference on Robotics and Automation (ICRA), 2016; pp.2846–2851. doi: 10.1109/ICRA.2016.7487448.

[17] Xie Y M, Andrew A. Two degree of freedom control synthesis with applications to agricultural systems. Journal of Dynamic Systems, Measurement, and Control, 2014; 136(5): 051006.

[18] Ahmadi I. Dynamics of tractor lateral overturn on slopes under the influence of position disturbances: Model development. Journal of Terramechanics, 2011; 48(5): 339–346.

[19] Qi W C, Li Y M, Tao J F. Design and Experiment of an active attitude adjustment system for tractors in hilly mountains. Transactions of the CSAM, 2019; 50(7): 381–388. (in Chinese)

[20] Sun J B, Chu G P, Pan G T, Meng C, Liu Z J, Yang F Z. Design and performance test of remote control omnidirectional leveling mountainous tracked tractors. Transactions of the CSAM, 2021; 52(5): 358–369. (in Chinese)

[21] Jin C Q, Yang T X, Liu G W, Wang T G, Chen M, Liu Z. Design and testing of omnidirectional leveling chassis for tracked combine harvesters. Transactions of the CSAM, 2020; 51(11): 393–402. (in Chinese)

[22] Liu G H, Hao C Y, Li M Z, Sun H. Design and simulation of posture control system for semi-active suspension mountain tractors. Transactions of the CSAM, 2022; 53(S2): 338–348. (in Chinese)

Liaoning University of Engineering and Technology, 2021; 95p. (in Chinese)